Journal of Medicinal Chemistry

pubs.acs.org/jmc

Article

Synthetic Peptides That Antagonize the Angiotensin-Converting Enzyme-2 (ACE-2) Interaction with SARS-CoV-2 Receptor Binding Spike Protein

Afsaneh Sadremomtaz, Zayana M. Al-Dahmani, Angel J. Ruiz-Moreno, Alessandra Monti, Chao Wang, Taha Azad, John C. Bell, Nunzianna Doti, Marco A. Velasco-Velázquez, Debora de Jong, Jørgen de Jonge, Jolanda Smit, Alexander Dömling, Harry van Goor,* and Matthew R. Groves*

Cite This: J. Med. Chem. 2022, 65, 2836−2847

Read Online

ACCESS | Metrics & More | Article Recommendations | Supporting Information

ABSTRACT: The SARS-CoV-2 viral spike protein S receptor-binding domain (S-RBD) binds ACE2 on host cells to initiate molecular events, resulting in intracellular release of the viral genome. Therefore, antagonists of this interaction could allow a modality for therapeutic intervention. Peptides can inhibit the S-RBD:ACE2 interaction by interacting with the protein−protein interface. In this study, protein contact atlas data and molecular dynamics simulations were used to locate interaction hotspots on the secondary structure elements α1, α2, α3, β3, and β4 of ACE2. We designed a library of discontinuous peptides based upon a combination of the hotspot interactions, which were synthesized and screened in a bioluminescence-based assay. The peptides demonstrated high efficacy in antagonizing the SARS-CoV-2 S-RBD:ACE2 interaction and were validated by microscale thermophoresis which demonstrated strong binding affinity (∼10 nM) of these peptides to S-RBD. We anticipate that such discontinuous peptides may hold the potential for an efficient therapeutic treatment for COVID-19.

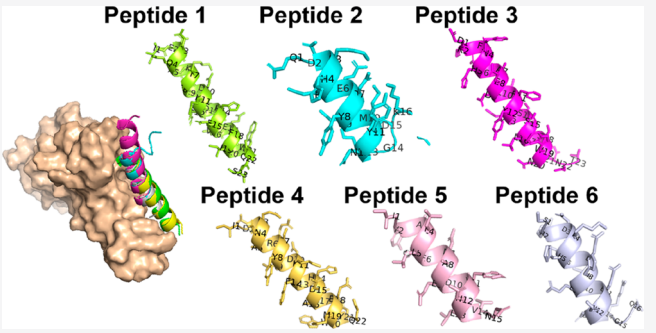

INTRODUCTION

To date, more than 100 coronaviruses have been discovered (https://www.who.int/emergencies/diseases/novel-coronavirus-2019/situation-reports/) and no targeted therapy yet exists for the current emergency of SARS-CoV-2 (COVID-19) infections. Scientists have applied many strategies against COVID-19, including assessing existing available antiviral drugs,[1] computationally screening for molecules,[2,3] designing compounds to block viral RNA synthesis/replication,[4−6] recognizing hotspot loops and residues to ligate the active axes of the virus by blocking binding to cognate human cell receptors,[7,8] using peptidomimetic reporters and identifying host specific receptors or enzymes to design specific drugs or vaccines,[9,10] targeting downstream host innate immune signaling pathways,[11] and performing computational genomic and pathological studies on different kinds of coronaviruses to design new drugs.[12−15]

There is a continuously evolving global effort to develop COVID-19 treatments or vaccines. Testing multiple approaches will improve the chance that a treatment is discovered. According to a WHO analysis of candidate COVID-19 vaccines, 64 are in clinical assessment (with 13 at phase 3) and 173 are in preclinical analyses. Phase 3 vaccine candidates include a variety of vaccine platforms: vector vaccines, mRNA-based vaccines, inactivated vaccines, and adjuvanted recombinant protein nanoparticles.[16−27]

The initial and critical route of entry of both SARS-CoV and SARS-CoV-2 viruses is the interaction between the viral S protein and ACE2 receptor. Therefore, impairing S-RBD binding to ACE2 has the potential to inhibit viral entry into human cells, presenting an opportunity for therapeutic intervention as a complement to vaccination strategies. While small molecules could disrupt the S-protein and ACE2 receptor interaction, they are suboptimal to target large protein−protein interactions (PPIs).[28−33] Antagonistic peptide drugs represent the best tool to inhibit the S-RBD:ACE2 interaction, as such peptides combine the best features of antibody approaches (ability to address a large and relatively featureless surface) and small-molecule approaches (improved pharmacokinetics, reduced immune response, ease of production, and cost of goods).[34−54]

Special Issue: COVID-19

Received: March 16, 2021
Published: July 30, 2021

https://doi.org/10.1021/acs.jmedchem.1c00477
J. Med. Chem. 2022, 65, 2836−2847

Table 1. Amino Acid Sequences of ACE2-Antagonist Peptides[a]

entry	sequence	m/z (monoisotopic) theor	m/z (monoisotopic) exptl	K_d (nM)	IC_{50} (nM)
peptide 1	H-IEEQAKTFLDKFQHEVEEIYWQS-NH_2	2895.397	2895.477	106 ± 1	11 ± 1
peptide 2	H-QDKHEEDYQMYNKGDKED-NH_2	2269.944	2270.011	102 ± 6	18 ± 2
peptide 3	H -DKFNHEAEDLFYQSSLASWNYNT-NH_2	2777.225	2777.304	245 ± 3	6 ± 4
peptide 4	H-IDENARSYIDKFQHDAEEMWYQ-NH_2	2786.228	2786.308	541 ± 5	32 ± 2
peptide 5	H-IYALLENAEDYNLVN-NH_2	1751.862	1751.920	13 ± 1	9 ± 4
peptide 6	H-SRDKHEEHEKENDRGQ-NH_2	1991.905	1991.966	46 ± 5	10 ± 5

[a]Theoretical and experimental molecular weight, half-maximal inhibitory concentration (IC_{50}) using a luciferase assay and binding affinities of SARS-CoV-2:ACE2-antagonist peptides (determined using) MST are also shown. Peptides were synthesized on solid phase using the F-moc strategy, have a free N-terminus, and are amidated at the C-terminus.

The interface between S-RBD and ACE2 has been recognized as a potential area for antagonism to inhibit viral propagation, and peptides derived from ACE2 have been used successfully to block SARS-CoV-2 cell entry.[48] The concept of utilizing discontinued peptides in drug discovery, and especially to combat SARS-CoV cell entry, was initiated decades ago with the discovery of the P6 peptide (EEQAKTFLDKFNHEAEDLFYQSS-G-LGKGDFR).[48] This peptide is derived from a library of peptides based on the α1 helix of ACE2. The P6 peptide is artificially linked by glycine that keeps two separate segments of ACE2 in close proximity and shows antiviral activity (IC_{50} = 0.1 mM).[48] This finding indicated that a core of S-RBD interacts with same α1 helix of ACE2. This approach is supported by recent publications that have suggested ACE2-based peptides as strong candidates for optimization into therapeutics[34−37] and is a complementary approach to vaccine development as well as the identification of small-molecule-based therapies (novel or repurposed). The strength of the interaction between ACE2 and S-RBD has been determined by a number of authors, indicating binding affinities of 94 and 44 nM by isothermal titration calorimetry (ITC) and surface plasmon resonance (SPR), respectively.[49,50] These figures provide an estimate for the required strength of interaction between any peptides and their target molecules that could reasonably be expected to antagonize the ACE2−S-RBD interaction, and ACE2-based peptide inhibitors of SARS-CoV-2[34−37] have recently been described. While this early stage of peptide inhibitor development showed great promise, only a few ACE-2-based peptides were proposed and screened, including SBP, a peptide that specifically binds S-RBD with micromolar affinity (1.3 μM) as assessed by biolayer interferometry.[34] A series of biosimilar peptides has recently been generated based on the N-terminal helix of human ACE2, which contains the majority of the residues at the binding interface, which displayed a high helical propensity. One of their most promising peptide-mimics (P10) blocked SARS-CoV-2 human pulmonary cell infection with an IC_{50} of 42 nM and 0.03 nM binding affinity (K_d), as assessed by biolayer interferometry.[36] A recent publication also reported that four stapled peptides show antiviral activity in HT1080/ACE2 cells (IC_{50} of 1.9 to 4.1 μM) and A549/ACE2 (IC_{50} of 2.2 to 2.8 μM).[37] The most promising of these peptides binds SARS-CoV-2 S-RBD with a K_d of 2.2 μM, as determined by SPR.

Additionally, a recent report describes the therapeutic effect of a tandem, lipidated peptide (1168-DISGINASWNIQKEID-RLNEVAKNLNESLIDLQEL-1203) from the heptad repeat (HRC) domain of SARS-CoV-2 in a ferret model.[39] This peptide has IC_{50} values of 303.1 nM in viral infection assays. However, the direct strength of interaction to the target S-RBD is unreported.[38] Further, a recently reported multiepitope peptide-based SARS-CoV-2 vaccine demonstrated high immunogenic response (IC_{50} of 2.4 μM and 9.0 μM for peptides 1 and 2, respectively). Finally, a defensin-like peptide P9R (NGAICWGPCPTAFRQIGNCGRFRVRCCRIR) displayed excellent activity against pH dependent viruses (IC_{50} of 0.26 nM).[40]

The availability of high-resolution structural information has facilitated this approach, by identifying the key interaction points between the two molecules of ACE2 and S-RBD (PDB: 6MOJ and 6M17).[51] However, the interaction strength of a single linear epitope of ACE2 is likely to be significantly inferior to that displayed by a composite peptide that is composed of disparate interaction epitopes. We have previously shown similar behavior in the design of a composite VEGF:VEGFR antagonistic peptide, that was shown to be competitive with an antibody-based approach in vitro and in vivo.[52−54] Similarly, the concatenation of disparate binding elements resulted in improved binding properties. This leads to the concept of a peptide-based therapeutic for the current SARS-CoV-2 outbreak, which would complement antibody-based approaches, but with the additional advantages of peptides over antibodies in terms of reduced cost-of-goods, immune response, ease of production, and improved pharmacokinetics. All of these issues are clearly of immense importance in developing therapeutics for the current outbreak.

In this paper, molecular docking and protein contact atlas[55−59] analysis revealed a number of interactions that are essential for the SARS-CoV-2 S-RBD:ACE2 interaction. Analyzing the S-RBD/ACE2 crystal structure (PDB ID: 6M0J and 6M17), and modeling the key interacting motifs of S-RBD with ACE2, we identified a number of hotspot loops distributed on the surface and thereby implicated as critical for virus entry into human cells. Analysis of this data resulted in a library of six peptides that we predicted would efficiently antagonize SARS-CoV-2 S-RBD:ACE2 interaction. This library was synthesized and assayed against an in vitro bioluminescence assay[60] to determine their inhibition of the SARS-CoV-2 S-RBD:ACE2 interaction. Our data below demonstrates that all six peptides were able to strongly compete for this interaction. While this approach clearly shows the efficacy of our peptides, we also performed microscale thermophoresis (MST) experiments to validate our proposed mode of inhibition, as well as to determine in vitro peptide binding affinities to purified SARS-CoV-2 S-RBD. The MST data indicates that a number of the peptides have binding affinities in the low nanomolar range with peptides 5 and 6 displaying affinities of 13 and 45 nM, respectively, which is

https://doi.org/10.1021/acs.jmedchem.1c00477
J. Med. Chem. 2022, 65, 2836−2847

Table 2. Table of Energetic Calculations Using HADDOCK[a]

entry	electrostatic energy score (arbitrary units of energy)	van der Waals energy score (arbitrary units of energy)	score	buried surface area ($A^{\bullet 2}$)	effect
peptide 1	−284.989 ± 2.3	−113.23 ± 1.1	−94.364 ± 7.2	927.565 ± 32	B
peptide 2	−386.163 ± 1.7	−127.31 ± 2.2	−104.789 ± 4.3	1024.23 ± 21	C
peptide 3	−272.940 ± 2.4	−111.43 ± 0.17	−93.334 ± 9.6	995.967 ± 34	B
peptide 4	−265.347 ± 1.1	−105.61 ± 0.9	−87.56 ± 3.5	1021.25 ± 29	B
peptide 5	−388.163 ± 4.2	−190.20 ± 1.4	−155.53 ± 9.2	1123.57 ± 37	D
peptide 6	−383.163 ± 3.3	−187.36 ± 1.9	−143.034 ± 10.13	1017.77 ± 41	D

[a]Effect; The experimentally determined effect on interaction of ACE2 with S-RBD. A: No effect on interaction with S-RBD. B: Slightly inhibits interaction with S-RBD. C: Strongly inhibits interaction with S-RBD. D: Abolishes interaction with S-RBD.

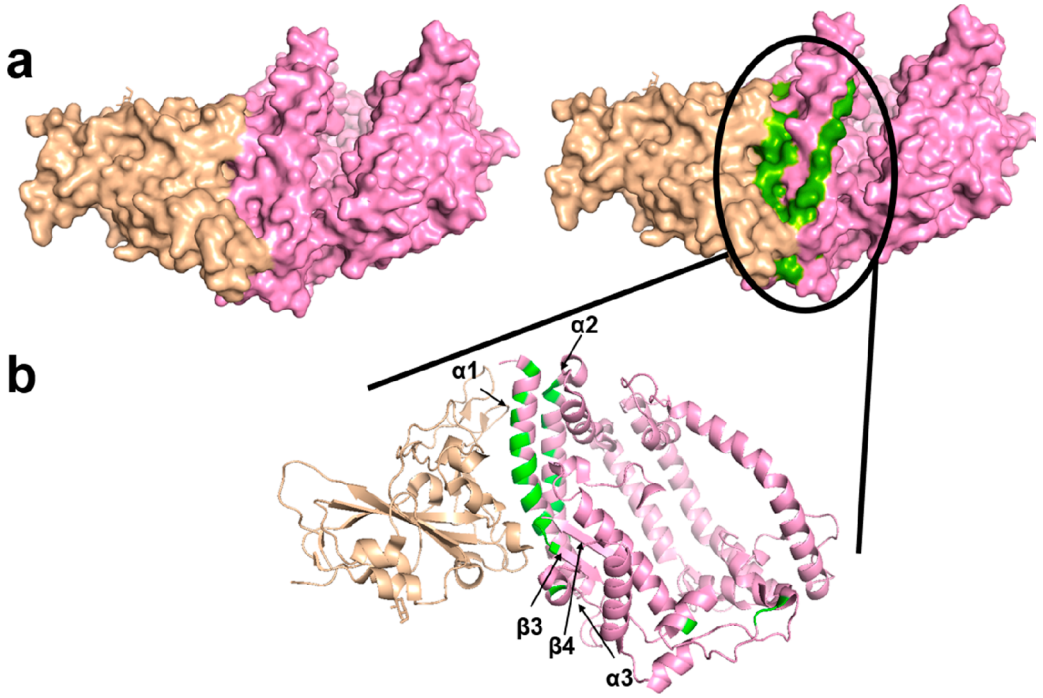

Figure 1. Interaction of ACE2 with S-RBD. (a) Surface representation of the complex between the receptor binding (S-RBD) domain of SARS-CoV-2 Spike protein (yellow) and the human ACE2 receptor (pink) (PDB ID: 6M0J). The portion of the ACE2 domain including main interacting residues of helices α1 (I21, Q24, T27, F28, D30, K31, H34, E35, E37, D38, Y41, Q42), α2 (L79, M82, Y83), and α3 (N330, K419, D430, E431) and β sheets β3 and β4 (K353, G354, D355, and R357) are drawn in green. (b) A closer view displays the interacting residues at the interface site. Figure created by PyMol (Molecular Graphics System, ver. 1.2r3pre, Schrödinger, LLC).

competitive with literature reported values of 0.03[36] and 1300 nM[34] binding affinity for P10 and SBP1 (ACE2 antagonist peptide), respectively.

In summary, this paper provides a clear indication that a composite peptide of ACE2, composed of loop elements that support the central interaction motif of its with S-RBD, can efficiently antagonize this essential interaction in vitro and provide the basis for further discovery of a COVID-19 therapeutic.

RESULTS AND DISCUSSION

Molecular Docking and Computational Modeling of ACE2:S-RBD Antagonistic Peptides. To identify key SARS-CoV-2 S-RBD:ACE2 interaction residues, protein−protein docking was performed using HADDOCK[61] and binding interfaces were predicted using protein contact atlas.[59] Additionally, we performed a structural analysis aiming to identify the S-RBD amino acids which energetically favor contacts with the ACE2 receptor by stabilizing a number of important interactions (Tables 1 and 2). The molecular interaction profile allowed us to identify the most frequent contacts between the peptides and S-RBD, suggesting these peptides may block the SARS-CoV-2 S-RBD:ACE2 axis by directly binding and inducing conformational changes in SARS-CoV-2 S-RBD (Figures 1 and 2).

Structural reports identified key 14 residues as important in the interaction of SARS-CoV S-RBD with ACE2[62] and revealed critical amino acid residues at the contact interface between S-RBD and full-length human ACE2 receptor. Analysis of 144 SARS-CoV-2 genome sequences available from GISAID (Global Initiative on Sharing All Influenza Data)[63] indicated that 8 of these 14 amino acids are strictly conserved (Table S1).

We first analyzed the interacting residues at the ACE2 and S-RBD interface using the crystal structures of ACE2 and S-RBD of SARS-CoV-2 (PDB: 6M0J and 6M17) and PDBePISA.[64] Fifteen residues of 23 residues (21−43) located on the α1 helix of ACE2 interact with S-RBD. These residues are clearly located in the crystal structure and include Q24, T27, D30, K31, H34, E35, E37, D38, Y41, and Q42 from helix α1, one

https://doi.org/10.1021/acs.jmedchem.1c00477
J. Med. Chem. 2022, 65, 2836−2847

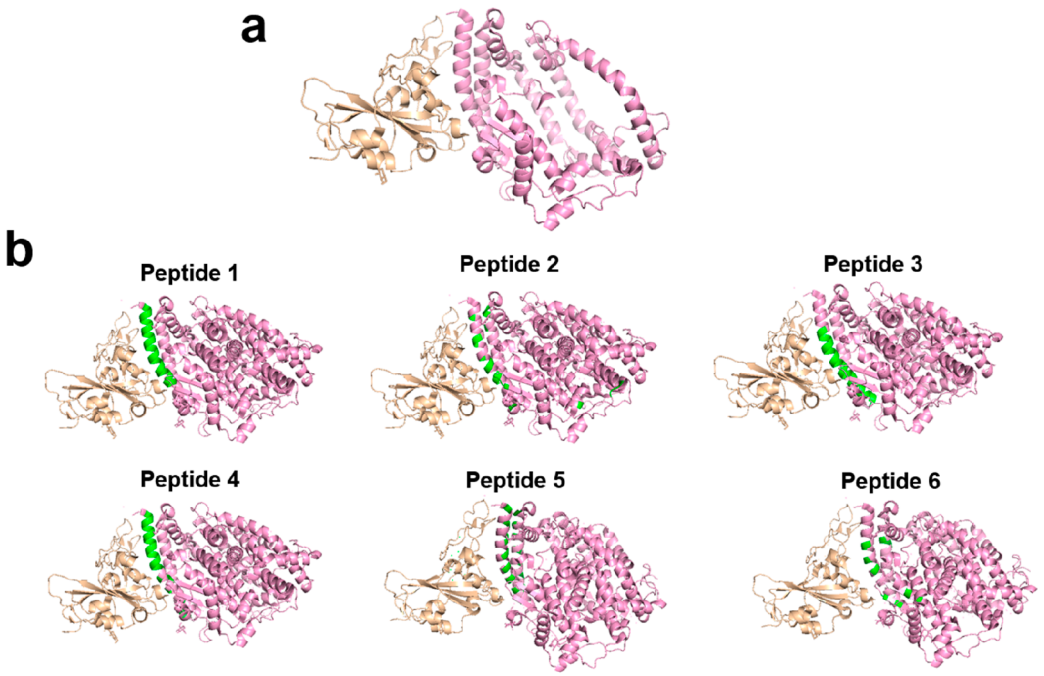

Figure 2. Stick representation of residues involved in the interprotomer interaction of S-RBD. (a) Side view of the surface representation of the interactions within ACE2 and S-RRBD (PDB ID: 6M0J). (b) Residues involved in the subunit interaction are shown in green (cartoon transparency is set to 40%). Four contact regions are located in the α1, α2and α3 helices and in β3 and β4 of ACE2 and S-RBD. Figure created by PyMol (Molecular Graphics System, ver. 1.2r3pre, Schrödinger, LLC).

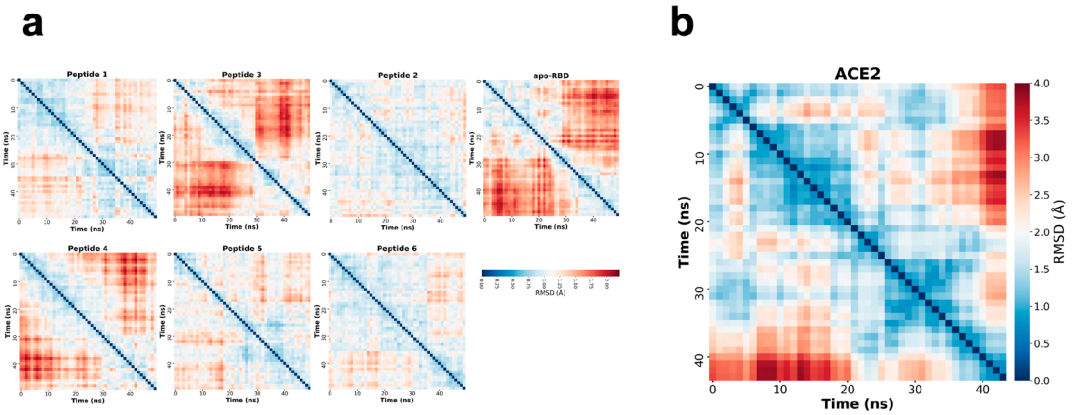

Figure 3. (a) Heat maps representing the pairwise backbone RMSD matrix of SARS-CoV-2 S-RBD protein calculated for the backbone along 50 ns of MD simulation from systems including peptides with stable binding to S-RBD. The unliganded protein (apo-RBD) is included for comparison. The simulation corresponding to apo-RBD displays a higher RMSD in comparison with the matrices originated for peptides 1, 2, 5, and 6. Indicating a less flexible conformation of S-RBD. (b) The unliganded protein (ACE2:S-RBD) is included for comparison

residue (M82) from helix α2, and residues K353, G354, D355, and R357 from the β3-β4 linker. Most of the interacting residues are located in α1 (Figures 1 and 2). Using the results from protein−protein molecular docking and the structural analysis, we assembled peptide 1, peptide 3, and peptide 4 from helix α1 alone (Table 1). The design strategy of peptide 2 is as a discontinuous peptide that includes some critical interacting amino acids from α1, α2, and α3 (330, 419, 430, and 431) and some key amino acids from residues between β3 and β4 (353 to 355), as shown in Figures 1, 2b and S1. However, a number of amino acids were identified as passenger residues and replaced with appropriate amino acids to preserve the binding energy (Figures 1, 2, and S1). Peptide 5 was again designed around helix α1, but to additionally include main interacting amino acids from helix α2 (V59, N63, D67, A71, E75, L79, and Y83). Finally, we designed a highly discontinuous peptide (peptide 6) including residues from α1, α2, and α3 helices and β4 that are known to bind to S-RBD (Figures 1, 2b, and S1b; Table S2).

We performed molecular docking experiments with the peptides and a model of SARS-CoV-2 S-RBD to characterize the binding of the designed peptides. All docking experiments showed that the peptides bind at the S-RBD surface in a manner similar to that of the α1 helix of ACE2. Furthermore, the analysis of binding by explicit solvent MD indicates that all peptides remained bound to S-RDB over the whole simulation. Importantly, the pairwise backbone RMSD analysis of four of the peptides showed a distinct profile to that generated by apo-S-RBD (Figure 3a). Binding of peptides 1, 2, 5, and 6 decreases the RMSD of the S-RBD backbone when compared with the

https://doi.org/10.1021/acs.jmedchem.1c00477
J. Med. Chem. 2022, 65, 2836−2847

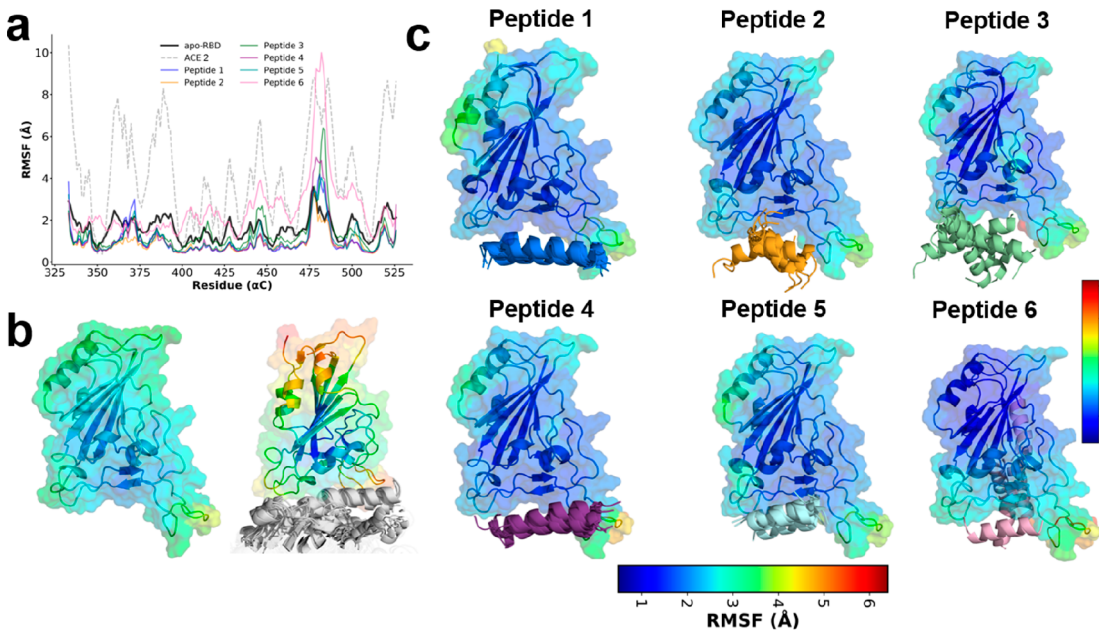

Figure 4. α-Carbon RMSF analysis for the peptide-S-RBD systems. (a) α-Carbon RMSF profiles of all studied peptides, apo-S-RBD, and ACE2 are presented for comparison. (b) RMSF structural representation of apo-S-RBD and ACE2:S-RBD. (c) structural representation of peptide:S-RBD complexes including the binding of the peptides across 10 representative snapshots. Normalized scale for peptides 1−5; peptide 6 is presented with its own scale.

apo structure (Figure 3). This induced transition might lead to a less flexible conformation of the protein, modulating the active state of the S-RBD protein and thus improving the affinity and the residence time of the peptides. The thermodynamic and kinetics of this conformational transition of ligand−receptor systems has been described previously.[65,66]

Additionally, a carbon alpha RMSF analysis of S-RBD (Figure 4) showed that most of peptides modified the fluctuations occurring in apo-S-RBD (Figure 4a). In particular, peptides 1−5 decreased the fluctuations among most of the residues. Notably, a considerable increase in RMSF values was observed on residues 469−488, comprising a flexible loop in proximity to the binding site of the peptides (Figure 4). This same loop has been described as containing key contacts for the interaction with the human ACE2 protein.[35,48] Moreover, we observed an overall RMSF change distribution on the S-RBD structure (Figure 4b and c). Although all peptides remain bound to S-RBD, peptide 6 displayed a nonunique binding mode. In the simulations, this peptide leaves the initial binding site and binds into different regions of S-RBD, causing a notable increment in S-RBD fluctuation (Figure 4c). Conversely, peptides 1, 4, and 5 are suggested to be the most stable binders, since they maintained a similar binding mode throughout the MD simulation (Figure 4c). Moreover, the molecular interactions profiles from MD indicated that peptides 1, 2, 4, and 5 formed high frequency interactions with the same residues where the helices α1 and α2 of ACE2 bind (Figure S1). On the other hand, peptide 3 showed lower frequency of interactions (Figure S1). Moreover, peptide 3 also showed a more variable binding mode (Figure 4c). Finally, peptide 6 showed a nonunique binding mode by exploring other regions of S-RBD (Figure 4c) as a consequence, the molecular interaction profile indicated the formation of interactions with several residues of the S-RBD protein (Figure S1a) including those of the SARS-CoV-2 S-RBD:ACE2 interface (Figure S1).

Interestingly, as shown in Table 2, peptides 1, 3, and 4 are closest in binding energies, likely as they are structurally similar and derived from helix α1 alone. Peptides 2, 5, and 6 have higher binding strength than the α-1 helix alone, in which the van der Waals and electrostatic interactions make a significant contribution (Table 2 and Figure S2). Taken together, these data suggest that the six designed peptides could bind SARS-CoV-2 S-RBD and induce a conformational change. Additionally, the MD interaction analysis suggested that the designed peptides would bind with a high affinity to S-RBD, with the exception of peptide 3. As a consequence, we decided to synthesize and evaluate their ability to antagonize the S-RBD:ACE2 interaction and their binding to a recombinant SARS-CoV-2 S-RBD (Figure S3).

Biophysical Characterization of Peptides of ACE2-Antagonist Peptides. Preliminary binding experiments between SARS-CoV-2 S-RBD protein domain and ACE2-antagonist peptides dissolved in PBS did not provide reproducible results (data not shown). We hypothesized that this is a result of poor aqueous solubility and/or aggregation phenomena of peptides in our experimental conditions. In line with this hypothesis, sequence analysis using the AGGRESCAN server (http://biocomp.chem.uw.edu.pl/A3D/)[67] suggested that all peptides, apart from peptides 4 and 6, show a propensity for self-aggregation (Figure S4).

Therefore, to identify experimental conditions for further assays, we performed a biophysical characterization of peptides. First, we comparatively assessed the solubility of peptides in PBS with and without additives such as Tween 20 and 1% (w/v) PEG8000, starting from the same stock solutions prepared in DMSO. We determined the difference between the experimental and the theoretical values as percentage of the theoretical values (% Error), for each solution tested. As reported in Table S3, a significant discrepancy between the experimental and theoretical values was observed in peptides dissolved in PBS compared to those

https://doi.org/10.1021/acs.jmedchem.1c00477
J. Med. Chem. 2022, 65, 2836−2847

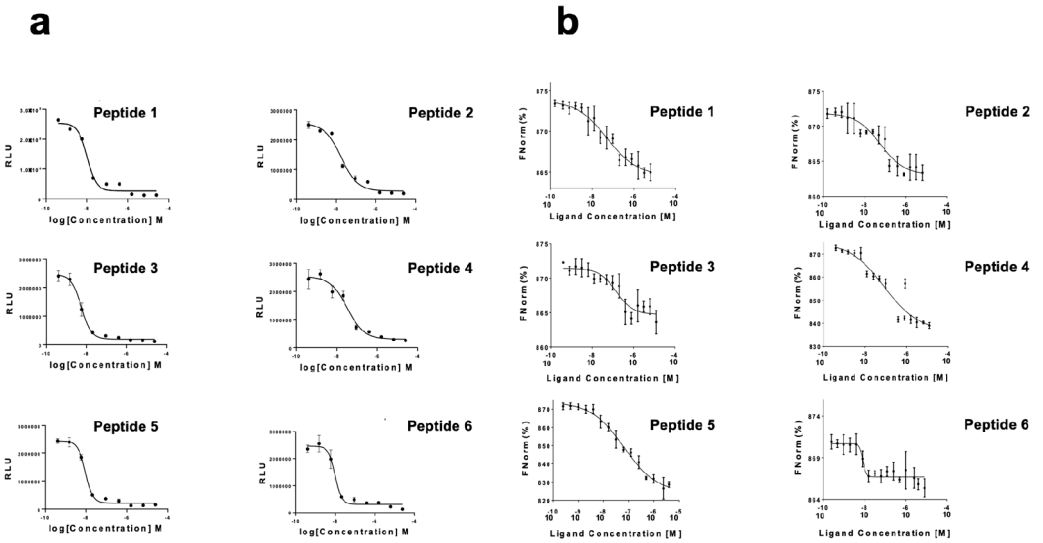

Figure 5. (a) Binding analysis for the interaction between S-RBD and ACE2. (a) Luciferase-based assay. 293T cells were transfected with the ACE2 or S-RBD expression constructs. 48 h post-transfection, and luciferase assays were performed on 20 μg total protein from cell lysates using FMZ as a substrate (n = 3, mean ± SD; one-way ANOVA, ***p < 0.005 relative to smBiT-ACE2 alone, Dunnett's correction for multiple comparisons). (b) MST analysis of peptide 1−6 binding to recombinant S-RBD. The concentration of S-RBD is kept constant at 50 nM, while the ligand concentration varies from 12.5 μM to 0.19 nM. Serial titrations result in measurable changes in the fluorescence signal within a temperature gradient that can be used to calculate the dissociation constant (K_d). The curve is shown as ΔFnorm (change of Fnorm with respect to the zero-ligand concentration) against S-RBD concentration on a log scale.

dissolved in PBST, 1% (w/v) PEG8000. As long as the analyzed solutions in PBS and PBST, 1% (w/v) PEG8000 were prepared from the same stocks, Tween and PEG8000 in PBS significantly increase the solubility of the peptides in solution. In our attempt to compare the solubility of peptides in PBST, 1% (w/v) PEG8000 used in this study, with respect to the PBS in the working concentrations (low micromolar range), we performed intrinsic fluorescence analysis following aromatic residues (Figure S5). Accordingly, we scanned the fluorescence emission spectra from 300 to 500 nm for peptides containing aromatic residues (Table 1).

As shown in Figure S5, the fluorescence emission increases linearly with peptide concentration for most peptides dissolved in PBST, 1% (w/v) PEG8000 and in PBS, indicating that peptides are soluble in the range of concentration tested. Differently, peptide 2 did not show a dose-dependent increase of fluorescence emission when dissolved in PBS compared to that dissolved in PBST, 1% (w/v) PEG8000. Indeed, a significant quenching of fluorescence emission is observed at the highest concentration tested (12.5 and 25 μM), suggesting that precipitation/aggregation phenomena or conformational changes occur in PBS. Of note, in all peptides tested, a quenching of fluorescence emission, primarily at the highest concentrations tested, has been observed in peptides dissolved in PBS compared to those dissolved in PBST, 1% (w/v) PEG8000 (Figure S6), suggesting different conformational behaviors of peptides in the two buffers used.

In this framework, the putative conformational changes of peptides in the two buffers has been evaluated using CD spectroscopy. The spectra of all peptides appeared disordered in PBS buffer, characterized with a strong peak minimum at 198 nm and a negative value at 190 nm, and showed more ordered structures, as detected by the appearance of a positive band at 190 nm and by the shift of the minimum from 198 to 205 nm, when dissolved in PBST, 1% (w/v) PEG8000 (Figure S7), suggesting that the presence of Tween and PEG8000 in the PBS better stabilizes the conformation of peptides.

Finally, the conformational behavior of peptides in the two buffers was further investigated by performing a comparative analysis with analytical size-exclusion chromatography (SEC) (see Experimental Section for details). Under the same experimental conditions, all peptides eluted as a single peak from the SEC column as observed in Figure S8. However, apart from peptide 1, all peptides showed a delayed retention time (Rt) when dissolved in PBS compared to those dissolved in PBST, 1% (w/v) PEG8000. Considering the apparent molecular weights of the synthetic peptides, calculated by a calibration curve, and their theoretical molecular weights, the number of the units of all peptides span in the range of 0.9−1.4 for peptides dissolved in PBST, 1% (w/v) PEG8000 and 0.3−0.9 for those dissolved in PBS (Figure S8). These data show that while all peptides are monomers in both buffers, they exhibit a more compact conformation in PBS with respect to that in PBST 1% (w/v) PEG8000. Conversely, peptide 1 showed a more open conformation in PBS with respect to that in PBST 1% (w/v) PEG8000. However, the elution peak in PBST, 1% (w/v) PEG8000 is very wide suggesting the presence of several conformation in solution.

Altogether these data show that no oligomerization are detectable in PBS or PBST, 1% (w/v) PEG8000. However, the presence of two surfactants increases the aqueous solubility of peptides and provides greater stabilization of the conformation of the peptides in solution. For these reasons, binding studies were performed using PBST, 1% (w/v) PEG8000 to solubilize the peptides.

Synthetic Peptides Efficiently Block the Interaction of ACE2 with S-RBD. The various ACE2 antagonist peptides identified above were synthesized and assessed for their ability to inhibit the S-RBD interaction with ACE2 using a luciferase assay (Figure 5a). Taha et al.[60] provides a novel bio-luminescence-based sensor reporter system, the reassembly

https://doi.org/10.1021/acs.jmedchem.1c00477
J. Med. Chem. 2022, 65, 2836−2847

of SmBiT and LgBiT into NanoBiT when S-RBD and ACE2 interact, to probe antagonism of the protein−protein interaction. This sensitive yet robust assay, developed for the discovery of neutralizing antibodies, allowed us to rapidly test peptide-based antagonism of the SARS-CoV-2 S-RBD:ACE2 interaction. Initially, we measured toxicity and inhibition of infection at nine concentrations (0−25 μM) of peptides, performed in triplicate (Figure 5a). We then used ACE2-antagonistic peptides to determine whether these peptides could disrupt the SARS-CoV-2 S-RBD:ACE2 interaction in a cell-based system. The reported half-maximal inhibitory concentration (IC_{50}) of our peptides against the SARS-CoV-2 S-RBD:ACE2 interaction demonstrates dose-dependent inhibition, with measured IC_{50}s of 11 ± 5, 18 ± 2, 6 ± 3, 32 ± 2, 9 ± 4, and 10 ± 3 nM against peptides 1−6, respectively (Table 1 and Figure 5a). At the highest concentrations used (25 μM), all peptides completely inhibited S-RBD binding to ACE2. At a concentration of 0.39 μM, peptides 2 and 4 exhibited up to ∼95% inhibition, and peptides 1, 3, 5, and 6 exhibited statistically significant inhibition of S-RBD binding at concentrations as low as 0.09 μM (Figure 5a).

Synthetic Peptides Bind to Purified S-RBD with Nanomolar Affinity. Microscale thermophoresis (MST) of the interaction of purified S-RBD with the six designed peptides was performed on a NanoTemper Monolith NT.115 (Nano Temper Technologies, Germany) and the results are shown in Figure 5b. To perform these experiments, pure S-RBD protein was labeled and incubated with a peptide concentration series (12.5−0.00019 μM) in PBS-Tween (0.01%) + 1% (w/v) PEG8000 (w/v). The addition of Tween and PEG8000 was necessary, as previous experiments in the absence of these reagents resulted in a high degree of aggregation of the peptide in the MST experiments. Triplicates of the thermophoretic progress curves are reported as the median of K_d posterior distribution for peptide 1 to peptide 6, showing values of 106 ± 1, 102 ± 6, 245 ± 3, 542 ± 5, 13 ± 1 and 46 ± 5 nM, respectively. Overall, all six peptides showed a sigmoid binding curve with K_d in the low nanomolar range, which indicate a strong binding of these peptides to the protein in a short incubation time (5 min). Results shown are mean ± SD of 3 measurements and are in close correlation with those of the luciferase assay (Figure 5b), in which peptides 5 and 6 also demonstrated the strongest antagonism (Figure 5b). Given the affinity of SARS-CoV-2 S-RBD to ACE2 has been reported as 44.2[49] and 94 nM[50] by SPR and ITC, respectively, these peptides clearly offer an opportunity to effectively inhibit viral cell entry in an in vivo settling.

In summary, the MST binding affinity experiments demonstrated that all peptides bind to SARS-CoV-2 S-RBD, and our MD data suggest that the noncontinuous design of peptide 6 might contribute to a nonunique binding mode allowing this peptide to bind similarly to helix1 and helix 2 of ACE2, but also including other proximal areas of S-RBD with a considerable enhancement of the binding affinity.

CONCLUSION

During an outbreak, conventional small molecule drug discovery[68−70] is perhaps not the most efficient option, as it cannot easily provide a sufficiently rapid solution. Several advantages over conventional small molecule drugs have been presented with peptide-based therapeutics, including elevated specificity and synthesis savings in both cost and time.[69,70] While this increased specificity is also accomplished by monoclonal antibodies,[45,60] they are expensive and labor-intensive to synthesize. There has also been some controversy over antibody mediated viral entry, which may lead to acute disease. Several approaches, such as drug repurposing, vaccination, and immunotherapy, represent reasonable alternatives. However, immunotherapy and vaccination approaches utilize peptide targets, and molecular dynamic simulations on the available X-ray crystal structure of the SARS-CoV-2 ACE2/S-RBD complex provided a straightforward way to identify potential peptide-based therapeutics.[69]

Several groups have reported peptides that recognize either ACE2 or SARS-CoV-2 S-RBD and inhibit virus from entering human cells in vitro and in vivo. Four SARS-BLOCK synthetic peptides were shown to inhibit SARS-CoV-2 spike protein-mediated infection of human ACE2-expressing cells LPDP-LKPTKRSFIEDLLFNKVTLADAGFMKQYG (K_d = 2 ± 1 μM), ASANLAATKMSECVLGQSKRVDFCGKGYH (K_d = 5 ± 2 μM), QILPDPSKPSKRSFIEDLLFNKVTLADAGFIK, ASANLAATKMSECVLGQSKRVDFCGKGY (K_d = 4 ± 2 μM), and ASANLAATKMSECVLGQSKRVDFCGKGY (K_d = 2 ± 2 μM).[44] To date, the most promising candidates of N-terminal ACE2 α1 helix-based peptides have been reported by a 27-mer peptide (aa 19−45)[36] and a 23-mer peptide (aa 21−43),[34] termed P10 and SBP1, respectively, which were shown to bind to S-RBD with a K_d of 0.03 nM and 1.3 μM, respectively, as assessed by biolayer interferometry. However, SBP1 binds to S-RBD which was expressed in insect cells, and the results were not reproduced with human and other insect-derived RBDs (provided from commercial sources).[34] This suggests that either the α1 helix of ACE2 is not sufficient to bind S-RBD or it loses its helical structure, and thereby its ability to bind S-RBD, in solution. This finding is in good agreement with recent reports,[34−37] and our luciferase and MST results for peptides 1−4 (Figure 5) have demonstrated that α1 alone might not be sufficiently stable to provide a sufficiently strong interaction. In accordance with this finding, Yanxiao et al.[35] reported initial computational findings that indicated an interaction between α1 and α2-helices may help retain their bent shape to match to the binding surface of SARS-COV-2 S-RBD, providing a more complete coverage of the S-RBD surface than the α1 helix alone. To provide additional confidence in the design of our peptide candidates, we compared the results of peptide 5 with peptide 1 (Figure 5). This follow-up comparison demonstrated that a candidate containing contributions from both α1 and α2 helices showed a more than 7-fold improvement in binding affinity to S-RBD, compared with other α1-helix-based peptides (peptide 1). Peptide 6 additionally comprises residues from three helices and β4 and shows similar levels of activity in the competition assay. It also demonstrated an ∼2-fold improvement in affinity over peptide 1 in binding affinity (Figure 5b). In summary, this indicates that helices α1 and α2 are likely closely packed together in the interaction of peptide 6 with SARS-CoV-2 S-RBD (Figures 1b and 2b), stabilizing each other to preserve structure as well as function.

Indeed, given the strong performance of our library of peptides with all ACE2- based peptides in the in vitro studies (12.9 and 45.9 nM for peptides 5 and 6, respectively), we believe that our peptides could provide a strong option for further drug development. However, our peptides derived from ACE2 are currently physiologically inactive as initial experiments on viral inhibition assays were unsuccessful (Table S3). Due to this lack of activity and the need to use surfactants

https://doi.org/10.1021/acs.jmedchem.1c00477
J. Med. Chem. 2022, 65, 2836−2847

(PEG8000 and Tween20), which are known to be cytotoxic in cell-based assays, we have also not performed cytotoxicity assays. Analysis of the solution properties of the peptides in this study clearly demonstrates a variation in peptide solubility and overall conformation in the absence or presence of these surfactants (Supporting Information), and modifications will need to be made to our peptides to translate the measured in vitro activity and binding affinity into activity in cell-based assays. However, similar difficulties have been previously reported in the design of S-RBD:ACE2 antagonistic peptides,[71−73] which were addressed by creating a tandem peptide, linked by a cholesterol moiety.[39] These experiments are currently underway and the results will be reported in a subsequent manuscript.

We believe that our data provides the first direct proof that, while the ACE2 α1 helix is an essential component for binding S-RBD, other loop regions such as helices α2, α3 and sheets β3, β4 of ACE2 also contribute significantly to the binding of SARS-CoV-2 S-RBD. We utilized a library of discontinues peptides to target S-RBD specifically and inhibit interaction of ACE2 with ACE2-S-RBD. Our study also further highlights the potential of a discontinuous peptide-based strategy in identifying antiviral drugs to target new mutations of S-RBD interactions which will undoubtedly offer an approach against future pandemics.

EXPERIMENTAL SECTION

Protein-Peptide Docking. The crystal structure of the S-RBD-ACE2 (PDB ID: 6M0J) complex was retrieved from the Protein Data Bank (https://www.rcsb.org/) and used as the starting point for the docking studies. Molecular docking was performed using the HADDOCK 2.4[61] server. The docking results were analyzed using the Chimera[74] and DS Visualizer programs. The results obtained were analyzed for binding energies and peptide conformations in the S-RBD binding interface. To identify hot-spot residues, we used Protein Contact Atlas (https://www.mrc-lmb.cam.ac.uk/rajini/index.html).[59] Briefly, we used a Chord Plot which shows the interactions between pairs of secondary structural elements (Figures 1 and 2), the adjacency matrix which reveals specific residue−residue interactions and represents the number of atomic contacts between them, an Asteroid Plot which shows the neighborhood of a particular residue or ligand, network statistics (Scatter Plot Matrix) which shows the network metrics corresponding to each residue (Closeness), statistics table that provides the degree, betweenness, and closeness centrality measures and solvated area of the selected residues), and the network view, in which interactions are represented as edges, with the edge thickness signifying the number of atoms that form contacts between the two residues).

Molecular Dynamics. MD simulations were performed using Gromacs 5.0.4.[55] The six designed peptides and S-RBD protein (6M0J) were parametrized using the CHARMM36 force field through the CHARMM-GUI (http://www.charmm-gui.org/).[56] For each peptide:S-RBD complex, the system was constructed by adding TIP3P water molecules, neutralizing ions, and establishing periodic boundary conditions (PBC) by using the multicomponent assembler of the CHARMM-GUI. Before production, the systems were minimized and then equilibrated under an NVT assembly. During the production phase, an NPT assembly was performed at 310.15 K for 50 ns saving velocities, and positions every 10 ps, and energy every 2 ps. Analysis of peptide-target interactions was computed by a python tailor-made script (https://github.com/AngelRuizMoreno/Scripts_Notebooks/blob/master/Scripts/plipMD_peptide_V1.1.py) using MDAnalysis[65] and PLIP.[66]

Free Energy Calculations. Full-length trajectories were employed for free energy calculations using the molecular mechanics energies combined with the Poisson−Boltzmann surface area continuum solvation (MM/PBSA)[68] by the g_mmpbsa v1.6 package.[69] Computation of the potential energy in vacuum, polar solvation energy, and nonpolar solvation energy were performed to calculate the average binding energy.

Peptide Synthesis and Characterization. Protected amino acids, coupling agents (HATU, Oxyma) used for peptide synthesis were purchased from Sigma-Aldrich (Milan, Italy) and Fmoc-Rink Amide MBHA LL resin was purchased from Novabiochem (Milan, Italy). Synthesis products, including acetonitrile (CH3CN), dimethylformamide (DMF), *N*,*N*′-diisopropylcarbodiimide (DIC), triisopropylsilane (TIS), trifluoroacetic acid (TFA), sym-collidine, diethyl-ether, and diisopropylethylamine (DIPEA), piperidine, were from Sigma-Aldrich (Milan, Italy). Peptides were assembled in the solid phase (Rink-Amide LL resin) with a substitution of 0.40 mmol/g, using a standard Fmoc peptide protocol with Oxyma-DIC and HATU-collidine as coupling reagents, as previously reported.[75] The cleavage of peptides from the solid support was performed by treatment with a TFA/TIS/H_2O (95:2.5:2.5, v/v/v) mixture for 3 h at room temperature. Crude peptides were precipitated in cold diethyl-ether, dissolved in a H_2O/CH_3CN (75:25, v/v) mixture and lyophilized. Purifications were performed at 15 mL/min using a Jupiter C18 (5 μm, 300 Å, 150 × 21.2 mm ID) column applying a linear gradient of 0.1% TFA in CH3CN from 1% to 80% over 15 min, and monitoring the absorbance at 210 nm.

ESI-TOF-MS analyses of crude and purified peptides were performed with an Agilent 1290 Infinity LC System coupled to an Agilent 6230 time-of-flight (TOF) LC/MS System (Agilent Technologies, Cernusco Sul Naviglio, Italy). The liquid chromatograph Agilent 1290 LC module was coupled with a photodiode array detector (PDA) and a 6230 time-of-flight MS detector, along with a binary solvent pump degasser, column heater and autosampler. The characterizations were performed at 0.2 mL/min using a XBridge C18 column (5 μm, 50 × 2,1 mm ID) applying a linear gradient of 0.1% TFA in CH_3CN from 1% to 80% over 10 min, and monitoring the absorbance at 210 nm. The relative purity of peptides was calculated as the ratio of peak area of the target peptide and the sum of areas of all detected peaks from the UV chromatograms. The purity of all peptides is more than 95% (Figure S3).

Determination of Peptide Concentrations. Peptide concentrations have been determined according to the Beer−Lambert law: $A = \varepsilon lc$, where A is the absorbace at 280 nm, ε is the molar absorption coefficient, and l is the cell path length, by using the Thermo Scientific NanoDrop 2000/2000c spectrophotometer (PerkinElmer, Monza Italy). The ε values at 280 nm have been calculated according to the equation: $\varepsilon_{280} = (5500n_{Trp}) + (1490n_{Tyr}) + (125n_{S-S})$, where the numbers are the molar absorbances for tryptophan (Trp), tyrosine (Tyr), and cystine (i.e., the disulfide bond, S−S), and n_{Trp} = number of Trp residues, n_{Tyr} = number of Tyr residuels, and n_{S-S} = number of disulfide bonds.[76] The concentration of peptide A6, lacking of aromatic residues, has been calculated via the Scopus Method, monitoring the absorbance at 205 nm.[77]

Intrinsic Fluorescence Analysis. Measurements of the intrinsic fluorescence emission in solution of peptides were performed on a Jasco model FP-750 spectrofluorophotometer in a 1.0 cm path length quartz cell. Peptides were dissolved in DMSO to obtain stock solutions at 1.0 mM. Working solutions (3.125, 6.25, 12.5, and 25 μM) were subsequently prepared starting from fresh solutions at 25 μM obtained from dilutions with PBS or PBST-1% (w/v) PEG8000 by the stocks of each peptide. After the dilution, all samples appeared clear, and the fluorescence emission was recorded in the 300−500 range upon excitation at 280 and 295 nm for peptides containing tyrosine and tryptophan, respectively. Each spectrum is the average of three scans corrected by subtraction of appropriate blank.

Circular Dichroism (CD) Measurements. Far-UV (190−260 nm) CD spectra were recorded on a Jasco J-715 spectropolarimeter, equipped with a PTC-423S/15 Peltier temperature controller, in a 0.1 cm path-length quartz cell, at 25 °C, as previously reported in the literature. Peptides were dissolved in 1,1,1,3,3,3-hexafluoro-2-propanol (HFIP) to obtain stock solutions at 1.0 mM and therefore diluted in PBS and PBST, 1% (w/v) PEG8000 at final concentration of 25 μM with 2.5% HFIP. Each spectrum is the average of three

https://doi.org/10.1021/acs.jmedchem.1c00477
J. Med. Chem. 2022, 65, 2836−2847

scans corrected by subtraction of appropriate blank. Intensities were expressed as mean residue ellipticity, the molar ellipticity per mean residue $[\theta] \times (\text{deg cm}^2\ \text{dmol}^{-1})$, obtained from the relation: $[\theta]222 = [\theta]\text{obs (mrw)}/(10cl)$, where $[\theta]$obs is the observed ellipticity in degree, "mrw" is the mean residue molecular weight of the protein, c is the protein concentration (g/mL), and l is the optical path length of the cell in cm.

Size-Exclusion Chromatography Experiments. Size-exclusion chromatography experiments were performed using an AKTA FPLC system (GE HEALTHCARE). Samples at about 10 mg/mL in DMSO were diluted in PBS and PBST, 1% (w/v) PEG8000 at a final concentration of 0.5 mg/mL, and 500 μL was loaded onto a BioSep-SEC-s2000 column 300 × 7.8 cm ID (Phenomenex), equilibrated with PBS at pH 7.0 at a flow rate of 0.5 mL/min. Chicken ovalbumin (44000 Da), myoglobin (16 900 Da), ribonuclease (13700 Da) and an unrelated peptide (ND, 2800 Da) were used as MW calibrants.

Plasmid Construction. Biosensors were cloned into the *Bam*HI/NotI sites of pcDNA3.1 to generate mammalian expression constructs.

Cell Culture. 293T (ATCC CRL-3216) were cultured in Dulbecco's modified Eagle's medium (Sigma) containing 10% FBS, and 1% penicillin/streptomycin (Invitrogen).[47]

In Vitro NanoLuc Assay. 293T cells (3×10^5 cells) were plated in 12-well plates in triplicate 24 h before transfection. An amount of 500 ng of the biosensor constructs was transfected using PolyJet transfection reagent (SignaGen Laboratories). After 48 h, supernatant or cells were collected. Cells were lysed using passive lysis buffer (Promega), and NanoLuc luciferase assays were performed using one of two substrates: furimazine, FMZ(Nano-Glo Cell Reagent, Promega) or native coelenterazine, CTZ (3.33 uM final concentration) (Nanolight Technologies – Prolume Ltd., Pinetop, AZ, USA). Synergy Microplate Reader (BioTek, Winooski, VT, USA) was used to measure luminescence. Results are presented as RLU (Relative Luminescence Unit) normalized to control. The data presented are the mean of three independent experiments.[47]

Microscale Thermophoresis (MST). The binding affinity of peptide to its cognate receptor was measured by Microscale thermophoresis (MST) on a Nanotemper Monolith NT.115 instrument (Nanotemper Technologies GmbH). Commercial S-RBD (RBD, FC Tag, 40592-v05H) was freshly labeled with the Monolith Lys-Tag RED-tris-NTA labeling dye according to the supplied protocol (Nanotemper Technologies, GmbH). The labeled protein was concentrated using a PES centrifugation filter (3 kDa cutoff; VWR). Measurements were done in MST buffer (50 mM Tris, 250 mM NaCl, pH = 7) in standard capillaries (K002; Nanotemper Technologies GmbH). The final concentrations of either labeled protein in the assay were 50 nM. The ligands (ACE2 peptides) were titrated in 1:1 dilution following manufacturer's recommendations and starting from 12.5 uM. All binding reactions were incubated for 5 min on ice followed by centrifugation at 20 000g before loading into capillaries. Then, samples were loaded into standard glass capillaries (Monolith NTCapillaries, Nano Temper Technologies) and the MST analysis was performed (settings for the light-emitting diode and infrared laser were 80%). All measurements were performed in triplicate using automatically assigned 20% LED and 50% MST power; Laser On-time was 30 s and Laser Off time was 5 s.

Statistical Analysis. All graphs and statistical analyses were generated using Excel or GraphPad Prism ver. 8. Means of two groups were compared using two-tailed unpaired Student's t test. Means of more than two groups were compared by one-way ANOVA with Dunnett's or Tukey's multiple comparisons correction. Alpha levels for all tests were 0.05, with a 95% confidence interval. Error was calculated as the standard deviation (SD). Measurements were taken from distinct samples. For all analyses, $^*P < 0.05$, $^{**}P < 0.01$, $^{***}P < 0.001$, $^{****}P < 0.0001$; n.s. = not significant. Data was reproduced by two different operators.

■ ASSOCIATED CONTENT

Supporting Information

The Supporting Information is available free of charge at https://pubs.acs.org/doi/10.1021/acs.jmedchem.1c00477.

Additional figures illustrating molecular interaction from MD analysis of designed peptides and S-RBD, binding free energy of ACE2 derived peptides in complexes of S-RBD (binding energies of ACE2:S-RBD included for comparison), peptide LC-MS characterization, details of changes in hot spot area plot caused by aggregation of peptides, variation of fluorescence peak intensity with increasing concentration of peptides, CD spectra of peptides, overlay of emission spectra of samples dissolved in PBS and PBST, 1% (w/v) PEG8000 at 25 μM in 2.5% DMSO, and SEC of peptides; additional tables detailing key interactions between S-RBD and ACE2 identified using PiPreD, peptide sequences including replacement of some residues for improved targeting of S-RBD, analysis of data collected for the calculation of concentration of peptides in PBS and PBST, 1% (w/v) PEG8000 by UV spectroscopy analysis, theoretical, apparent molecular weight, and Rt values of ACE2-antagonist peptides as determined by SEC analysis, and dose–response results of the antiviral activity of peptides in a SARS-CoV-2 infection inhibition assay performed in VERO-E6 cells (PDF)

■ AUTHOR INFORMATION

Corresponding Authors

Matthew R. Groves – *XB20 Drug Design, Groningen Research Institute of Pharmacy, University of Groningen, 9700 AD Groningen, The Netherlands*; orcid.org/0000-0001-9859-5177; Email: m.r.groves@rug.nl

Harry van Goor – *Department of Medical Microbiology and Infection Prevention, University of Groningen, University Medical Center Groningen, 9700RB Groningen, The Netherlands*; Email: h.van.goor@umcg.nl

Authors

Afsaneh Sadremomtaz – *XB20 Drug Design, Groningen Research Institute of Pharmacy, University of Groningen, 9700 AD Groningen, The Netherlands*

Zayana M. Al-Dahmani – *XB20 Drug Design, Groningen Research Institute of Pharmacy, University of Groningen, 9700 AD Groningen, The Netherlands; Department of Medical Microbiology and Infection Prevention, University of Groningen, University Medical Center Groningen, 9700RB Groningen, The Netherlands*

Angel J. Ruiz-Moreno – *XB20 Drug Design, Groningen Research Institute of Pharmacy, University of Groningen, 9700 AD Groningen, The Netherlands; Departamento de Farmacología, Facultad de Medicina, Universidad Nacional Autónoma de Mexico (UNAM), Ciudad de Mexico 04510, Mexico; Unidad Periférica de Investigación en Biomedicina Translacional, Facultad de Medicina, Universidad Nacional Autónoma de México (UNAM), Ciudad de Mexico 03229, Mexico; Doctorado en Ciencias Biomédicas, Universidad Nacional Autónoma de México (UNAM), Ciudad de Mexico 04510, Mexico*

Alessandra Monti – *Institute of Biostructures and Bioimaging (IBB)-CNR, 80134 Napoli, Italy*

Chao Wang − *XB20 Drug Design, Groningen Research Institute of Pharmacy, University of Groningen, 9700 AD Groningen, The Netherlands*
Taha Azad − *Center for Innovative Cancer Therapeutics, Ottawa Hospital Research Institute, Ottawa K1H 8L6 ON, Canada; Department of Biochemistry, Microbiology and Immunology, University of Ottawa, Ottawa K1H 8M5 ON, Canada*
John C. Bell − *Center for Innovative Cancer Therapeutics, Ottawa Hospital Research Institute, Ottawa K1H 8L6 ON, Canada; Department of Biochemistry, Microbiology and Immunology, University of Ottawa, Ottawa K1H 8M5 ON, Canada*
Nunzianna Doti − *Institute of Biostructures and Bioimaging (IBB)-CNR, 80134 Napoli, Italy*
Marco A. Velasco-Velázquez − *Departamento de Farmacología, Facultad de Medicina, Universidad Nacional Autónoma de Mexico (UNAM), Ciudad de Mexico 04510, Mexico; Unidad Periférica de Investigación en Biomedicina Translacional, Facultad de Medicina, Universidad Nacional Autónoma de México (UNAM), Ciudad de Mexico 03229, Mexico; Doctorado en Ciencias Biomédicas, Universidad Nacional Autónoma de México (UNAM), Ciudad de Mexico 04510, Mexico;* orcid.org/0000-0001-9717-0265
Debora de Jong − *Department of Medical Microbiology and Infection Prevention, University of Groningen, University Medical Center Groningen, 9700RB Groningen, The Netherlands*
Jørgen de Jonge − *Centre for Infectious Disease Control, National Institute for Public Health and the Environment (RIVM), 3720BA Bilthoven, The Netherlands*
Jolanda Smit − *Department of Medical Microbiology and Infection Prevention, University of Groningen, University Medical Center Groningen, 9700RB Groningen, The Netherlands;* orcid.org/0000-0001-6951-1448
Alexander Dömling − *XB20 Drug Design, Groningen Research Institute of Pharmacy, University of Groningen, 9700 AD Groningen, The Netherlands;* orcid.org/0000-0002-9923-8873

Complete contact information is available at: https://pubs.acs.org/10.1021/acs.jmedchem.1c00477

Author Contributions

A.S. conceived and designed a library of ACE2 peptides. A.S. implemented computational design pipelines and performed docking protocols and conducted data analyses. A.S. and Z.A. carried out MST experiments. A.J.R.-M., M.A.V.-V., and A.D. implemented MD computational studies and conducted data analyses. A.M. and N.D. provided the ACE2 peptide library and their biophysical characterization. C.W. supported the luciferase assay analysis. T.A. and J.B. engineered ACE2 and S-RBD luciferase construct. D.D.J. and J.D.J. carried out cell assay and performed viral transduction. A.S. wrote the paper, with input from all coauthors. A.S.S.D., M.G., and H.V.G. supervised the work. All coauthors reviewed the paper and provided critical insight and ideas.

Notes

The authors declare the following competing financial interest(s): A.S., M.G., H.V.G., A.M., and N.D. have filed a US patent application entitled on the "Synthetic peptides that block SARS-CoV-2" described in this paper.

■ ACKNOWLEDGMENTS

This research was supported by private funding by the University of Groningen and University Medical Center Groningen. Support from the project PRIN2017 Prot. 2017M8R7N9 is gratefully acknowledged. Computational studies have implemented by a grant from Universidad Nacional Autónoma de México (UNAM) supercomputer "Miztli" (LANCAD-UNAM-DGTIC-386 2020-2021) and Ph.D. scholarship of A.J.R-M. as a doctoral student from Programa de Doctorado en Ciencias Biomédicas, UNAM with fellowship 584534 from CONACYT.

■ ABBREVIATIONS

ACE2, angiotensin-converting Enzyme 2; ANOVA, Analysis of variance; CD, circular dichroism; CH_3CN, acetonitrile; CTZ, coelenterazine; DMF, dimethylformamide; DIC, *N*,*N*′-diisopropylcarbodiimide; DIPEA, diisopropylethylamine; ESI-TOF-MS, electrospray ionization time-of-flight mass spectrometry; FMZ, furimazine; ITC, isothermal titration Calorimetry; IC_{50}, half-maximal inhibitory concentration; LC/MS, liquid chromatography−mass spectrometry; mRNA, messenger RNA; MD, molecular dynamics; PPI, protein−protein interaction; PBS, phosphate-buffered saline; PEG, polyethylene glycol; PBC, periodic boundary conditions; PDA, photodiode array detector; RNA, ribonucleic acid; RMSD, root-mean-square deviation; RMSF, root-mean-square fluctuation; RLU, relative luminescence unit; SARS-CoV-2, severe acute respiratory syndrome coronavirus 2; S-RBD, spike-receptor binding domain; SPR, surface plasmon resonance; SD, standard deviation; TIS, tri-isopropylsilane; TFA, trifluoroacetic acid; TOF, time-of-flight; VEGF, vascular endothelial growth factor; VEGFR, vascular endothelial growth factor receptor; WHO, World Health Organization

■ REFERENCES

(1) Liu, C. H.; Lu, C. H.; Wong, S. H.; Lin, L. T. Update on antiviral strategies against COVID-19: unmet needs and prospects. *Front. Immunol.* **2021**, *11*, 616595.
(2) Galindez, G.; Matschinske, J.; Rose, T. D.; Sadegh, S.; Salgado-Albarrán, M.; Späth, J.; Baumbach, J.; Pauling, J. K. Lessons from the COVID-19 pandemic for advancing computational drug repurposing strategies. *Nat. Comput. Sci.* **2021**, *1*, 33−41.
(3) Hufsky, F.; Lamkiewicz, K.; Almeida, A.; Aouacheria, A.; Arighi, C.; et al. Computational strategies to combat COVID-19: useful tools to accelerate SARS-CoV-2 and coronavirus research. *Briefings Bioinf.* **2021**, *22*, 642−663.
(4) V'kovski, P.; Kratzel, A.; Steiner, S.; Stalder, H.; Thiel, V. Coronavirus biology and replication: implications for SARS-CoV-2. *Nat. Rev. Microbiol.* **2021**, *19*, 155−170.
(5) Zhang, L.; Lin, D.; Sun, X.; Curth, U.; Drosten, C.; Sauerhering, L.; Becker, S.; Rox, K.; Hilgenfeld, R. Crystal structure of SARS-CoV-2 main protease provides a basis for design of improved α-ketoamide inhibitors. *Science* **2020**, *368*, 409−412.
(6) Jin, Z.; Du, X.; Xu, Y.; Deng, Y.; Liu, M.; Zhao, Y.; Zhang, B.; Li, X.; Zhang, L.; Peng, C.; Duan, Y.; Yu, J.; Wang, L.; Yang, K.; Liu, F.; Jiang, R.; Yang, X.; You, T.; Liu, X.; Yang, X.; Bai, F.; Liu, H.; Liu, X.; Guddat, L. W.; Xu, W.; Xiao, G.; Qin, C.; Shi, Z.; Jiang, H.; Rao, Z.; Yang, H. Structure of M^{pro} from SARS-CoV-2 and discovery of its inhibitors. *Nature* **2020**, *582*, 289−293.
(7) Hussain, S.; Xie, Y. J.; Li, D.; Malik, S. I.; Hou, J. C.; Leung, E. L.; Fan, X. X. Current strategies against COVID-19. *Chin. Med.* **2020**, *15*, 70.
(8) Choudhary, S.; Malik, Y. S.; Tomar, S. Identification of SARS-CoV-2 cell entry inhibitors by drug repurposing using *in silico*

structure-based virtual screening approach. *Front. Immunol.* **2020**, *11*, 1664.
(9) Shyr, Z. A.; Gorshkov, K.; Chen, C. Z.; Zheng, W. Drug discovery strategies for SARS-CoV-2. *J. Pharmacol. Exp. Ther.* **2020**, *375*, 127−138.
(10) Gil, C.; Ginex, T.; Maestro, I.; Nozal, V.; Barrado-Gil, L.; Cuesta-Geijo, M.Á.; Urquiza, J.; Ramírez, D.; Alonso, C.; Campillo, N. E.; Martinez, A. COVID-19: drug targets and potential treatments. *J. Med. Chem.* **2020**, *63*, 12359−12386.
(11) Catanzaro, M.; Fagiani, F.; Racchi, M.; Corsini, E.; Govoni, S.; Lanni, C. Immune response in COVID-19: addressing a pharmacological challenge by targeting pathways triggered by SARS-CoV-2. *Signal Transduct Target Ther.* **2020**, *5*, 84.
(12) Wu, C.; Liu, Y.; Yang, Y.; Zhang, P.; Zhong, W.; Wang, Y.; Wang, Q.; Xu, Y.; Li, M.; Li, X.; Zheng, M.; Chen, L.; Li, H. Analysis of therapeutic targets for SARS-CoV-2 and discovery of potential drugs by computational methods. *Acta Pharm. Sin. B* **2020**, *10*, 766−788.
(13) VanPatten, S.; He, M.; Altiti, A.; F Cheng, K.; Ghanem, M. H.; Al-Abed, Y. Evidence supporting the use of peptides and peptidomimetics as potential SARS-CoV-2 (COVID-19) therapeutics. *Future Med. Chem.* **2020**, *12*, 1647−1656.
(14) Smith, M. C.; Gestwicki, J. E. Features of protein-protein interactions that translate into potent inhibitors: topology, surface area and affinity. *Expert Rev. Mol. Med.* **2012**, *14*, 14−16.
(15) Josephson, K.; Ricardo, A.; Szostak, J. W. mRNA display: from basic principles to macrocycle drug discovery. *Drug Discovery Today* **2014**, *19*, 388−99.
(16) WHO. *Draft landscape of COVID-19 candidate vaccines*. https://www.who.int/news-room/q-a-detail/coronavirus-disease-(covid-19)-vaccines (accessed January 2021).
(17) Voysey, M.; Clemens; Madhi, S.; Weckx, L. Y.; Folegatti, P. M.; et al. Safety and efficacy of the ChAdOx1 nCoV-19 vaccine (AZD1222) against SARS-CoV-2: an interim analysis of four randomised controlled trials in Brazil, South Africa, and the UK. *Lancet* **2021**, *397*, 99−111.
(18) Polack, F. P.; Thomas, S. J.; Kitchin, N.; et al. Safety and efficacy of the BNT162b2 mRNA Covid-19 vaccine. *N. Engl. J. Med.* **2020**, *383*, 2603−2615.
(19) Baden, L. R.; El Sahly, H. M.; Essink, B.; et al. Efficacy and safety of the mRNA-1273 SARS-CoV-2 vaccine. *N. Engl. J. Med.* **2021**, *384*, 403−416.
(20) Kovyrshina, A. V.; Dolzhikova, I. V.; Grousova, D. M.; et al. A heterologous virus-vectored vaccine for prevention of middle east respiratory syndrome induces long protective immune response against MERS-CoV. *Immunologiya* **2020**, *41*, 135−43.
(21) Logunov, D. Y.; Dolzhikova, I. V.; Zubkova, O. V.; et al. Safety and immunogenicity of an rAd26 and rAd5 vector-based heterologous prime-boost COVID-19 vaccine in two formulations: two open, non-randomised phase 1/2 studies from Russia. *Lancet* **2020**, *396*, 887−97.
(22) Logunov, D. Y.; Dolzhikova, I. V.; Shcheblyakov, D. V.; Tukhvatulin, A. Safety and efficacy of an rAd26 and rAd5 vector-based heterologous prime-boost COVID-19 vaccine: an interim analysis of a randomised controlled phase 3 trial in Russia. *Lancet* **2021**, *397*, 671.
(23) WHO. *Transmission of SARS-CoV-2: implications for infection prevention precautions*. https://www.who.int/news-room/commentaries/detail/transmission-of-sars-cov-2-implications-for-infection-prevention-precautions (accessed January 2020).
(24) Centers for disease control and prevention. *Interim clinical guidance for management of patients with confirmed coronavirus disease (COVID-19)*. https://www.cdc.gov/coronavirus/2019-ncov/hcp/ (accessed May 2020).
(25) WHO. *Target product profiles for COVID-19 vaccines*, 2020. https://www.who.int/publications/m/item/who-target-product-profiles-for-covid-19-vaccines (accessed January 2020).
(26) Amanat, F. K. SARS-CoV-2 vaccines: status report. *Immunity* **2020**, *52*, 583.
(27) Chen, W. H.; Strych, U.; Hotez, P. J.; Bottazzi, M. E. The SARS-CoV-2 vaccine pipeline: an overview. *Curr. Trop Med. Rep.* **2020**, *7*, 61.
(28) Leader, B.; Baca, Q. J.; Golan, D. E. Protein therapeutics: a summary and pharmacological classification. *Nat. Rev. Drug Discovery* **2008**, *7*, 21−39.
(29) Suntharalingam, G.; Perry, M. R.; Ward, S.; Brett, S. J.; Panoskaltsis, N.; et al. Cytokine storm in a phase 1 trial of the anti-CD28 monoclonal antibody TGN1412. *N. Engl. J. Med.* **2006**, *355*, 1018−1028.
(30) Wadman, M. London's disastrous drug trial has serious side effects for research. *Nature* **2006**, *440*, 388−389.
(31) Huck, B. R.; Kötzner, L.; Urbahns, K. Small molecules drive big improvements in immuno-oncology therapies. *Angew. Chem., Int. Ed.* **2018**, *57*, 4412−4428.
(32) Gadek, T. R.; Burdick, D. J.; McDowell, R. S.; Stanley, M. S. Generation of an LFA-1 antagonist by the transfer of the ICAM-1 immunoregulatory epitope to a small molecule. *Science* **2002**, *295*, 1086−1089.
(33) Scott, D. E.; Bayly, A. R.; Abell, C.; Skidmore, J. Small molecules, big targets: drug discovery faces the protein-protein interaction challenge. *Nat. Rev. Drug Discovery* **2016**, *15*, 533−550.
(34) Zhang, G.; Pomplun, S.; Loftis, A. R.; Loas, A.; Pentelute, B. L. Investigation of ACE2 N-terminal fragments binding to SARS-CoV-2 spike RBD. *bioRxiv*, June 17, **2020**, ver. 1. DOI: 10.1101/2020.03.19.999318.
(35) Han, Y.; Král, P. Computational design of ACE2-based peptide inhibitors of SARS-CoV-2. *ACS Nano* **2020**, *14*, 5143−5147.
(36) Karoyan, P.; Vieillard, V.; Gómez-Morales, L.; et al. Human ACE2 peptide-mimics block SARS-CoV-2 pulmonary cells infection. *Commun. Biol.* **2021**, *4*, 197.
(37) Curreli, F.; Victor, S. M. B.; Ahmed, S.; Drelich, A.; et al. Stapled peptides based on human angiotensin-converting enzyme 2 (ACE2) potently inhibit SARS-CoV-2 infection in vitro. *mBio* **2020**, *11*, No. e02451-20.
(38) Tai, W.; et al. Identification of SARS-CoV RBD-targeting monoclonal antibodies with cross-reactive or neutralizing activity against SARS-CoV-2. *Antiviral Res.* **2020**, *179*, 104820.
(39) De Vries, R. D.; Schmitz, K. S.; Bovier, F. T. Intranasal fusion inhibitory lipopeptide prevents direct contact SARS-CoV-2 transmission in ferrets. *bioRxiv*, November 5, **2020**, ver. 1. DOI: 10.1101/2020.11.04.361154.
(40) Tai, W.; He, L.; Zhang, X.; Pu, J.; Voronin, D.; Jiang, S.; Zhou, Y.; Du, L. Characterization of the receptor-binding domain (RBD) of 2019 novel coronavirus: implication for development of RBD protein as a viral attachment inhibitor and vaccine. *Cell. Mol. Immunol.* **2020**, *17*, 613−620.
(41) Sun, C.; Chen, L.; Yang, J. SARS-CoV-2 and SARS-CoV spike-RBD structure and receptor binding comparison and potential implications on neutralizing antibody and vaccine development. *bioRxiv*, February 20, **2020**, ver. 1. DOI: 10.1101/2020.02.16.951723.
(42) Xia, S.; Yan, L.; Xu, W.; Agrawal, A. S.; Algaissi, A.; Tseng, C. K.; Wang, Q.; Du, L.; Tan, W.; Wilson, I. A.; Jiang, S.; Yang, B.; Lu, L. A pan-coronavirus fusion inhibitor targeting the HR1mdomain of human coronavirus spike. *Sci. Adv.* **2019**, *5*, No. eaav4580.
(43) Rathod, S. B.; Prajapati, P. B.; Punjabi, L. B.; Prajapati, K. N.; Chauhan, N.; Mansuri, M. F. Peptide modelling and screening against human ACE2 and spike glycoprotein RBD of SARS CoV 2. *In Silico Pharmacol.* **2020**, *8*, 3.
(44) Watson, A.; Ferreira, L.; Hwang, P.; Xu, J.; Stroud, R. Peptide antidotes to SARS-CoV-2 (COVID-19). *bioRxiv*, August 6, **2020**, ver. 1. DOI: 10.1101/2020.08.06.238915.
(45) Singh, A.; Thakur, M.; Sharma, L. K.; Chandra, K. Designing a multi epitope peptide based vaccine against SARS CoV 2. *Sci. Rep.* **2020**, *10*, 16219.
(46) Molina, R.; Oliva, B.; Fernandez-Fuentes, N. A collection of designed peptides to target SARS-Cov-2 − ACE2 interaction: PepI-

Covid19 database. *bioRxiv*, April 29, **2020**, ver. 1. DOI: 10.1101/2020.04.28.051789.
(47) Zhao, H.; To, K. K. W.; Sze, K. H.; Yung, T. T.; Bian, M.; Lam, H.; Yeung, M. L.; Li, C.; Chu, H.; Yuen, K. Y. A broad-spectrum virus- and host-targeting peptide against respiratory viruses including influenza virus and SARS-CoV-2. *Nat. Commun.* **2020**, *11*, 4252.
(48) Han, D. P.; Penn-Nicholson, A.; Cho, M. W. Identification of critical determinants on ACE2 for SARS-CoV entry and development of a potent entry inhibitor. *Virology* **2006**, *350* (1), 15−25.
(49) Shang, J.; Ye, G.; Shi, K.; Wan, Y.; Luo, C.; Aihara, H.; Geng, Q.; Auerbach, A.; Li, F. Structural basis of receptor recognition by SARS-CoV-2. *Nature* **2020**, *581*, 221−224.
(50) Zhou, T.; Tsybovsky, Y.; Gorman, J.; Rapp, M.; Cerutti, G.; et al. Cryo-EM structures of SARS-CoV-2 spike without and with ACE2 reveal a pH-dependent switch to mediate endosomal positioning of receptor-binding domains. *Cell Host Microbe* **2020**, *28* (6), 867−879.
(51) Lan, J.; Ge, J.; Yu, J.; Shan, S.; Zhou, H.; Fan, S.; Zhang, Q.; Shi, X.; Wang, Q.; Zhang, L.; Wang, X. Structure of the SARS-CoV-2 spike receptor-binding domain bound to the ACE2 receptor. *Nature* **2020**, *581*, 215−220.
(52) Sadremomtaz, A.; Ali, A. M.; Jouyandeh, F.; Balalaie, S.; Navari, R.; et al. Molecular docking, synthesis and biological evaluation of vascular endothelial growth factor (VEGF) B based peptide as antiangiogenic agent targeting the second domain of the vascular endothelial growth factor receptor 1 (VEGFR1D2) for anticancer application. *Sig. Transduct. Target Ther.* **2020**, *5*, 76.
(53) Sadremomtaz, A.; Mansouri, K.; Alemzadeh, G.; Safa, M.; Rastaghi, A. E.; Asghari, S. M. Dual blockade of VEGFR1 and VEGFR2 by a novel peptide abrogates VEGF driven angiogenesis, tumor growth, and metastasis through PI3K/ AKT and MAPK/ ERK1/2 pathway. *Biochim. Biophys. Acta, Gen. Subj.* **2018**, *1862*, 2688−2700.
(54) Sadremomtaz, A.; Kobarfard, F.; Mansouri, K.; Mirzanejad, L.; Asghari, S. M. Suppression of migratory and metastatic pathways via blocking VEGFR1 and VEGFR2. *J. Recept. Signal Transduction Res.* **2018**, *38*, 432−441.
(55) Abraham, M. J.; Murtola, T.; Schulz, R.; Pall, S.; Smith, J. C.; Hess, B.; Lindahl, E. GROMACS: High performance molecular simulations through multi-level parallelism from laptops to supercomputers. *SoftwareX.* **2015**, *1* (2), 19−25.
(56) Jo, S.; Kim, T.; Iyer, V. G.; Im, W. CHARMM-GUI: a web-based graphical user interface for CHARMM. *J. Comput. Chem.* **2008**, *29*, 1859−1865.
(57) Gowers, R. J.; Linke, M.; Barnoud, J.; Reddy, T. J. E.; Melo, M. N.; Seyler, S.; et al. MDanalysis: a python package for the rapid analysis of molecular dynamics simulations. *Proceedings of the 15th python in science conference* **2016**, 98−105.
(58) Salentin, S.; Schreiber, S.; Haupt, V. J.; Adasme, M. F.; Schroeder, M. PLIP: fully automated protein−ligand interaction profiler. *Nucleic Acids Res.* **2015**, *43*, W443−W447.
(59) Kayikci, M.; Venkatakrishnan, A. J.; Scott-Brown, J.; et al. Visualization and analysis of non-covalent contacts using the protein contacts atlas. *Nat. Struct. Mol. Biol.* **2018**, *25*, 185−194.
(60) Azad, T.; Singaravelu, R.; Taha, Z.; Boulton, S.; et al. Nanoluciferase complementation-based biosensor reveals the importance of N- linked glycosylation of SARS-CoV-2 spike for viral entry. *Mol. Ther.* **2021**, *29*, 1984.
(61) Spiliotopoulos, D.; Kastritis, P. L.; Melquiond, A. S.; Bonvin, A. M.; Musco, G.; Rocchia, W.; Spitaleri, A. dMM-PBSA: A new HADDOCK scoring function for protein-peptide docking. *Front Mol. Biosci.* **2016**, *3*, 46.
(62) Li, W.; Zhang, C.; Sui, J.; Kuhn, J. H.; Moore, M. J.; Luo, S.; Wong, S. K.; Huang, I. C.; Xu, K.; Vasilieva, N.; Murakami, A.; He, Y.; Marasco, W. A.; Guan, Y.; Choe, H.; Farzan, M. Receptor and viral determinants of SARS-coronavirus adaptation to human ACE2. *EMBO J.* **2005**, *24*, 1634−1643.
(63) Elbe, S.; Buckland-Merrett, G. Data, disease and diplomacy: GISAID's innovative contribution to global health. *Global Challenges* **2017**, *1*, 33.
(64) Baskaran, K.; Duarte, J. M.; Biyani, N.; Bliven, S.; Capitani, G. A PDB-wide, evolution-based assessment of protein-protein interfaces. *BMC Struct. Biol.* **2014**, *14*, 1422.
(65) Amaral, M.; Kokh, D. B.; Bomke, J.; Wegener, A.; Buchstaller, H. P.; Eggenweiler, H. M.; et al. Protein conformational flexibility modulates kinetics and thermodynamics of drug binding. *Nat. Commun.* **2017**, *8*, 2276.
(66) Ferina, J.; Daggett, V. Visualizing protein folding and unfolding. *J. Mol. Biol.* **2019**, *431*, 1540−1564.
(67) Zambrano, R.; Jamroz, M.; Szczasiuk, A.; Pujols, J.; Kmiecik, S.; Ventura, S. AGGRESCAN3D (A3D): server for prediction of aggregation properties of protein structures. *Nucleic Acids Res.* **2015**, *43*, W306−313.
(68) Goel, B.; Bhardwaj, N.; Tripathi, N.; Jain, S. K. Drug discovery of small molecules for the treatment of COVID-19: a review on clinical studies. *Mini-Rev. Med. Chem.* **2021**, *21*, 1431.
(69) Pant, S.; Singh, M.; Ravichandiran, V.; Murty, U. S. N.; Srivastava, H. K. Peptide-like and small-molecule inhibitors against COVID-19. *J. Biomol. Struct. Dyn.* **2021**, *39*, 2904.
(70) Di Natale, C.; La Manna, S.; De Benedictis, I.; Brandi, P.; Marasco, D. Perspectives in peptide-based vaccination strategies for syndrome coronavirus 2 pandemic. *Front. Pharmacol.* **2020**, *11*, 578382.
(71) Pessi, A.; Bixler, S. L.; Soloveva, V.; Radoshitzky, S.; Retterer, C.; et al. Cholesterol-conjugated stapled peptides inhibit Ebola and Marburg viruses in vitro and in vivo. *Antiviral Res.* **2019**, *171*, 104592.
(72) Li, C. G.; Tang, W.; Chi, X. J.; Dong, Z. M.; Wang, X. X.; Wang, X. J. A cholesterol tag at the N terminus of the relatively broad-spectrum fusion inhibitory peptide targets an earlier stage of fusion glycoprotein activation and increases the peptide's antiviral potency in vivo. *J. Virol.* **2013**, *87*, 9223−9232.
(73) Pessi, A. Cholesterol-conjugated peptide antivirals: a path to a rapid response to emerging viral diseases. *J. Pept. Sci.* **2015**, *21*, 379−386.
(74) Pettersen, E. F.; Goddard, T. D.; Huang, C. C.; Couch, G. S.; Greenblatt, D. M.; Meng, E. C.; Ferrin, T. E. UCSF chimera–a visualization system for exploratory research and analysis. *J. Comput. Chem.* **2004**, *25*, 1605−1612.
(75) Caporale, A.; Doti, N.; Monti, A.; Sandomenico, A.; Ruvo, M. Automatic procedures for the synthesis of difficult peptides using oxyma as activating reagent: A comparative study on the use of bases and on different deprotection and agitation conditions. *Peptides* **2018**, *102*, 38−46.
(76) Grimsley, G. R.; Pace, C. N. Spectrophotometric Determination of Protein Concentration. *Curr. Protoc. Protein Sci.* **2003**, 3.1.1−3.1.9.
(77) Scopes, R.K. Measurement of protein by spectrophotometry at 205 nm. *Anal. Biochem.* **1974**, *59*, 277−282.

https://doi.org/10.1021/acs.jmedchem.1c00477
J. Med. Chem. 2022, 65, 2836−2847